Density functional analysis of key energetics in metal homoepitaxy: Quantum size effects in periodic slab calculations

Da-Jiang Liu
Ames Laboratory, U.S. DOE, Iowa State University, Ames, Iowa 50011, USA
(Received 22 May 2009; revised manuscript received 19 October 2009; published 15 January 2010)

Adspecies terrace diffusion barriers, pair interaction energies, and formation energies control island nucleation and growth during deposition and postdeposition coarsening in metal homoepitaxial systems. Thus, accurate theoretical determination of such energies is key for predicting behavior or for interpreting experiments. Often energies are obtained from density-functional theory using slab geometries. However, we find surprisingly strong variation in these energies with slab thickness due to quantum size effects, and also slow convergence to the bulk limit. Thus, many previously reported values deviate significantly from bulk limit, a feature corrected in the current study focusing on Ag and Cu surfaces.

DOI: 10.1103/PhysRevB.81.035415 PACS number(s): 68.35.Md, 71.15.Nc, 73.21.Fg, 81.10.Aj

I. INTRODUCTION

Density functional theory (DFT) analysis is proving to be an invaluable tool providing energetic information for either modeling or interpreting growth and relaxation behavior in epitaxial metal films.[1] DFT is having a similar impact on other areas of surface and materials science.[2] It is well recognized that there are intrinsic limitations to the reliability of the theory due to approximation of exchange-correlation functional in the Kohn-Sham equation. However, there are also more practical limitations for periodic slab calculations due to the use of finite-size (lateral) unit cells and due to finite-thickness slabs. It is common for such analyses to use slab thickness from $L=4-6$ layers for studies involving adsorption on one side of the slab (and perhaps double that for adsorption on both sides). The assumption is that this will be sufficient to recover $L\rightarrow\infty$ bulk behavior. However, the current analysis reveals unexpectedly strong quantum size effects (QSE) in the direction orthogonal to the slab. Values of key energies determined from slabs of thickness in the above regime deviate significantly from bulk values, and convergence to these values is surprisingly slow.

To explore this behavior, we focus on three key energies: the terrace diffusion barrier, E_d, the pair interaction, E_b, and the formation energy, E_f, for adatoms on fcc(100) and fcc(111) surfaces. We also discuss the adsorption energy, E_a, for adatoms, and both E_d and E_f for vacancies. Immediately below, we provide some brief background on the significance of the first three quantities for thin-film growth and relaxation processes.

For submonolayer deposition at low temperatures (T) where the formation of two-dimensional (2D) adatom islands is irreversible (i.e., ad-dimers are stable), island density, $N_{\rm isl}$, is controlled by E_d (in the absence of longer-range repulsive interactions between adatoms). A simple mean-field rate-equation treatment captures this dependence allowing determination of E_d from observations of the T dependence of $N_{\rm isl}$.[3,4] Increasing T results in a transition to reversible island formation which is controlled in large part by E_b. A mean-field estimate of the dependence of the transition temperature, T^*, on E_b (and E_d) comes from comparing the rate of dimer dissociation with the rate at which adatoms aggregate with dimers (noting that the latter creates larger more stable islands).[5] More precise determination of T^* accounts for frequent recombination of dissociating dimers.[3,4] Traditionally, E_b was determined from experimental values of T^*. However, sometimes experimental behavior is unclear, particularly if complicated by a distinct transition associated with the onset of dimer mobility.[6,7] Reliable DFT estimates of E_b facilitate correct interpretation of such experimental observations.

Similar issues arise for analysis of multilayer growth in the presence of a large step-edge barrier inhibiting downward transport and producing wedding-cakelike mounds (i.e., three-dimensional stacks of 2D islands).[3,4] The size of the uppermost terraces or islands in these mounds is extremely sensitive to the rate of nucleation of new layers on these terraces. This in turn is sensitive to the extent of reversibility in island formation and thus to E_b.[8] Behavior of the upper terrace size was first described by a mean-field treatment of the rate of nucleation of top-layer islands,[9] although subsequent analysis indicated distinct behavior in cases where nucleation was impacted by fluctuations in the adatom population of the top terrace.[10,11] In any case, precise values of E_b are key for modeling and elucidating these complex multilayer film morphologies.[8]

In addition, we briefly describe key energetic issues for postdeposition coarsening of 2D islands or pits via Ostwald ripening (OR). OR involves transport of adspecies (which could be either adatoms or vacancies) between islands or pits.[12,13] The overall coarsening rate is controlled by the sum of E_d and the effective energy, E_f, for forming adspecies on the terrace by detachment from steps edges (plus any additional barrier for attachment of adspecies to step edges). E_d is generally expected to be quite different for adatoms and vacancies. E_f would be the same for adatoms and vacancies within a simple nearest-neighbor (NN) pairwise interaction picture, although many-body aspects of the interactions produce differences.[13] Thus, reliable determination of E_f (as well as E_d) enables assessment of coarsening pathways and rates.

Finally, it should be noted that DFT analysis of energetics for (unsupported) thin metal slabs does have potential direct relevance to behavior on supported films, particularly when

there is a weak interaction of the film with the supporting substrate. Indeed, some studies of supported films on highly oriented pyrolytic graphite have been performed specifically to test this hypothesis.[14]

Earlier DFT studies on key energetics of simple metal surfaces also reveal significant variations due to the choice of slab thickness in calculations.[15–18] Given the importance of precise energetics for interpreting and modeling experiments, these observations prompt a more systematic and comprehensive study of quantum size effects exploiting enhanced computing power and refinements of theory and codes. The results will also be helpful in clarifying fundamental and practical issues related to the convergence of *ab initio* energetics as a function of slab thickness.

The outline of this paper is as follows. In Sec. II, we briefly describe the methodology and some details of the settings in our DFT calculations. In Sec. III, we present and discuss the results for nearest-neighbor interactions between adatom pairs. We present results for the formation energy in Sec. IV, and for the diffusion barrier in Sec. V, for both adatoms and vacancies. Discussion and conclusions are provided in Sec. VI.

II. METHOD

DFT results presented here are obtained using the VASP code.[19–22] Most of the calculations were performed with the Perdew-Burke-Ernzerhof (PBE) exchange-correlation functional[23] and the projector-augmented wave (PAW) method.[24,25] The pseudopotential is from the VASP package and tailored for PBE functional.[25] Methfessel and Paxton's smearing (with $N=1$ and $\sigma=0.2$ eV) were used for all slab calculations. The energy cutoff is 250 eV for all metals. For those calculations with relaxation, we fixed the bottommost layer atoms at their bulk positions and relax the upper layers, including adsorbates, if any. Slabs are separated by a vacuum of 12 Å. The settings for the k-point grid will be given in the main text. Theoretical lattice constants are obtained with $(24\times24\times24)$ k-point grid, including the Γ point, using the tetrahedron method with Blöchl corrections. They are 4.169 Å for Ag and 3.637 Å for Cu. The experimental lattice constant for Ag with the zero-point anharmonic expansion subtracted is calculated recently as 4.056 Å in Ref. 26 and 4.062 Å in Ref. 27, and the value for Cu is 3.595 and 3.596 Å, respectively. The room-temperature value is 4.09 Å for Ag and 3.61 Å for Cu.[28]

The overestimate of the lattice constant is a general feature of the PBE (and the very similar PW91) form of the generalized-gradient approximation (GGA) of DFT and is consistent with other previous GGA results, e.g, 4.17 Å (PW91+LAPW),[29] 4.18 Å (PW91, PP),[15] 4.13 Å (PBE, gaussian-type orbitals (GTO)),[30] 4.164 Å (PBE, PP) (Ref. 31) 4.147–4.150 Å (PBE, PAW),[32,33] and 4.154 Å (PAW, FP-(L)APW+lo).[32] The FP-(L)APW+lo value is considered the benchmark. The small but not insignificant difference with the (PBE, PAW) values in Refs. 32 and 33 is believed to be caused mainly by the difference in the PAW potentials used.[34] Similarly, the lattice constant for Cu is also consistent with previously reported values using PBE, e.g., 3.637 Å (PAW),[33] 3.630 Å [FP-(L)APW+lo],[32] and 3.628 Å (PBE and linear combination of atomic orbitals).[26] Results using other functionals and pseudopotentials are discussed in Appendix.

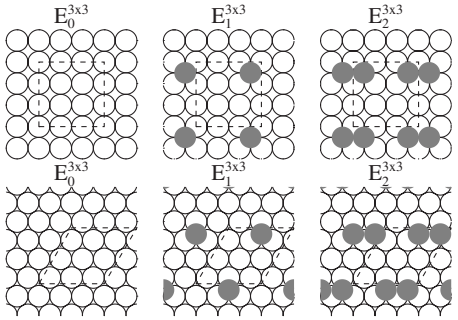

FIG. 1. Configurations used in the calculation of NN bond interactions for (100) (top panel) and (111) (bottom panel). Supercells of size (3×3) are shown here. Open circles are the topmost substrate atoms and the gray circles are adatoms. The surface unit cells are plotted as dashed lines.

It is sometimes tempting to use the experimental lattice constant to "correct" the theory. However, using a lattice constant that is different from the theoretical value will introduce an artificial strain to the system. As shown in Refs. 16 and 25 and will be discussed in Sec. V, the diffusion barrier is very sensitive to the strain but less sensitive to the "wrong" lattice constant caused by the limitation of the theory. We will be consistently using the theoretical lattice constant in the following sections, unless specified otherwise.

III. NEAREST-NEIGHBOR PAIR INTERACTIONS

To extract NN lateral interactions, E_b, between adatoms from *ab initio* energy calculations, we operate under the assumption that interactions beyond a certain range (e.g., two or three times the surface lattice constants) can be ignored. This is usually well justified.[36,37] Thus, comparison of the energetics of a neighboring pair of adsorbates on a surface with that for a far-separated pair within a large unit cell would produce the desired NN interaction. However, for (111) surfaces of noble metals, indirect interaction mediated by a Shockley surface state can extend to large distances,[38–44] and this would require use of an inordinately large unit cell. Unfortunately, in order to calculate energetics for a large range of slab thicknesses with the goal of systematically studying quantum size effects, we are restricted to relatively small supercells (less than 25 atoms per layer). Thus, to estimate the binding energy, $E_b>0$, for a NN adatom dimer, instead we use the following method.

For each slab thickness L, we compute the total energy of three configurations using a $(m\times m)$ supercell; the clean slab without any adsorbate [total energy $E_0^m(L)$]; with one adatom at fourfold hollow site for (100) surfaces, and at a threefold hollow fcc site for (111) surfaces [total energy $E_1^m(L)$]; and with a NN dimer, its constituent adatoms occupying the same type of sites as for the single atom case [total energy $E_2^m(L)$]. These three types of configurations are illustrated in Fig. 1

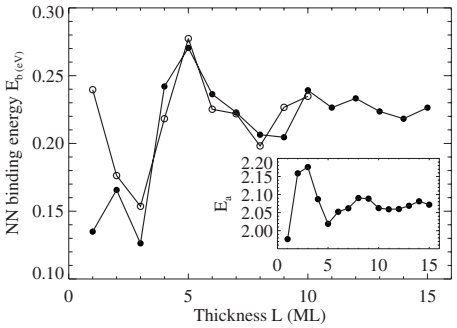

FIG. 2. NN adatom interaction energy for Ag(100) thin films. Solid circles are results derived using (3×3) supercells with a (8×8) k-point grid, and the open circles are derived using (4×4) supercells with a (4×4) k-point grid. The adatom adsorption energy E_a as a function of L in a (3×3) supercell is plotted as an inset.

for a (3×3) unit cell. In the following analysis, we will ignore all interactions longer than $m-1$ atomic distances or surface lattice constants (denoted by "a" below), i.e., we ignore interactions between adspecies in adjacent unit cells. Then, if $E_a(L)>0$ denotes the adsorption energy of an isolated adatom, and again $E_b(L)>0$ is the NN binding energy, for estimates from a slab of thickness L, we have the following relations:

$$E_1^m(L) = E_0^m(L) - E_a(L) \tag{1}$$

and

$$E_2^m(L) = E_0^m(L) - 2E_a(L) - E_b(L). \tag{2}$$

Consequently, E_a and E_b can then be obtained from

$$E_a(L) = E_0^m(L) - E_1^m(L),$$

$$E_b(L) = 2E_1^m(L) - E_0^m(L) - E_2^m(L). \tag{3}$$

A. Ag(100) and Cu(100)

The NN interaction energy for a dimer on a free-standing Ag(100) thin slab of thickness L was obtained using Eq. (3) with $m=3$ and a (8×8) k-point grid. Results are plotted in Fig. 2. This interaction ranges from 0.13 eV for $L=3$ to a maximum of 0.27 eV for $L=5$. Also, $L=10$ produces a slightly stronger interaction than nearby L values. Thus, a repeat period of five atomic layers can be discerned, as discussed further below.

Results using a larger (4×4) supercell with (4×4) k-point grid show very similar behavior. See also Fig. 2. For $L=1-10$, the mean absolute difference between results for E_b with $m=3$ and $m=4$ is 0.022 eV. Much of this difference is likely due to insufficient number of k points used for the calculation with $m=4$. Thus, for Ag(100), longer-range interactions beyond two atomic distances (around 6 Å) are negligible compared with the NN binding energy.

For completeness, in the inset of Fig. 2, we show the dependence on slab thickness, L, of the adsorption energy E_a. The variation with L is similar to that for E_b.

TABLE I. NN bond interactions, derived from Eq. (3) and average over slab thickness from $L=8$ to $L=15$. The uncertainties are estimated from the standard deviation of the data divided by the number of samples.

	(3×3) supercell		(4×4) supercell	
	Fixed	Relaxed	Fixed	Relaxed
Ag(100)	0.271(2)	0.222(2)		0.221(4)
Ag(111)	0.288(2)	0.231(2)	0.285(1)	0.225(2)
Cu(100)	0.369(1)	0.322(4)		
Cu(111)	0.331(2)	0.274(2)	0.319(1)	0.239(2)

Such dependence on film thickness of E_b (and E_a) is expected to be caused by the confinement of electrons along the direction perpendicular to the film. This results in a discretization of the energy band into quantum-well states (QWSs). This proposed presence of QSE is consistent with and supported by a number of observations. First, calculations without any relaxation (i.e., all atoms, including adsorbates, are fixed at their bulk positions) show similar behavior, although overall the pair interaction is increased by about 0.06 eV. Second, examination of the calculated electronic energy levels within unrelaxed clean slabs shows that one QSW (at $k_x=k_y=0$) crosses the Fermi level between $L=4$ and $L=5$, and another one crosses the Fermi level just below $L=10$, consistent with results by Wei and Chou.[45] A simple perspective of Schulte's analyses of QSE using a jellium model[46] is that such a crossing of the Fermi energy and a QWS results in a cusp in many physical quantities if the height of the film can be adjusted continuously. A free-electron analysis indicates that such crossing occurs approximately every five layers for Ag(100) and Cu(100) assuming one valence electron for each atom.[47]

What is perhaps surprising is the magnitude of the variation in E_b. For contrast, consider the surface energy (per atom), E_s, which governs relative stabilities of Ag(100) slabs for various thicknesses. For a slab thickness from $L=4$ to 10, which is usually consider thick enough to mimic bulk properties, the variation in E_s is around 0.01 eV for Ag(100). In contrast, the variance in E_b for this range of film thickness is much larger at around 0.07 eV. As an aside, a much larger variation is found in E_s for Ag(110).[47]

To extract the bulk value for E_b, we simply average the value for the larger range of thicknesses from $L=8$ to 15. More sophisticated method taking into account a propensity for period five oscillatory decay could, in principle, be employed. However, considering the irregularities in the DFT results (mainly caused by an insufficient number of k points and to a lesser extent by the finite-energy cutoff), there is likely not much benefit in so doing. The result from simple averaging for Ag(100) of 0.222 eV using a (3×3) supercell is listed in Table I, along with other results for this and similar systems.

There is also a significant additional advantage in considering an average value of E_b over several slab thicknesses rather than the value for a single thickness (even when it is very large). We find that from empirical evidence that

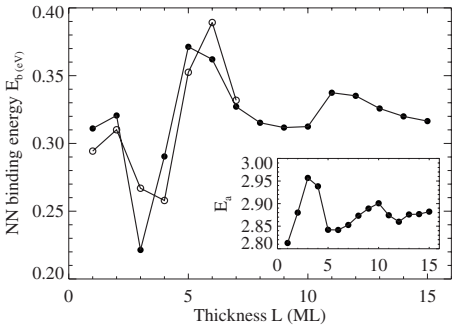

FIG. 3. NN adatom interaction energy for Cu(100) thin films. Solid circles are derived using (3×3) supercells with a (6×6) k-point grid, and open circles are results using (4×4) supercells and a (4×4) k-point grid. The adatom adsorption energies E_a for different slab thickness L in (3×3) supercells are plotted in the inset.

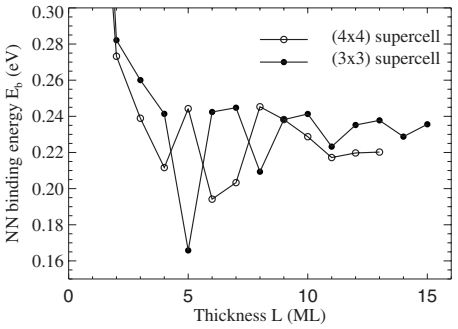

FIG. 4. NN pair interaction between Ag adatom on Ag(111). The solid circles are derived from using (3×3) supercells with a (8×8) k-point grid. The open circles are derived from using (4×4) supercells and a (4×4) k-point grid.

achieving k-point convergence is quite difficult on a slab of fixed thickness. For example, using (3×3) supercells, the absolute difference in E_b estimated with (6×6) and (8×8) k-point grids is 16 meV on average for $L=8$ to 15. However, the difference in the values averaged over this range is only 3 meV.

Behavior of E_b (and E_a) for Cu(100) as a function of slab thickness is quite similar to that for Ag(100), as shown in Fig. 3. Specifically, using a (3×3) supercell, we estimate that $E_b=0.22$ eV for $L=3$ ML and $E_b=0.37$ eV for $L=5$ ML. The bulk value obtained as the average value over $L=8$ to $L=15$ is 0.322 eV. We have carried out calculations for larger unit cells only for a range of smaller slab thickness L. However, we expect that as for Ag(100), results for E_b are not very sensitive to the lateral size of the supercell as long as it is above (3×3). Figure 3 also shows an oscillation with a period near 5–6 ML, suggesting the source of QSE in this system is due to the same quantum confinement effect as in Ag(100).

B. Ag(111) and Cu(111)

We can use the same method as for fcc(100) surfaces [i.e., Eq. (3)] to extract the NN adatom interaction energy for Ag(111) and Cu(111) slabs. Results using a (3×3) supercell with (8×8) k-point grid and a (4×4) supercell with (4×4) k-point grid are presented in Fig. 4. For a fixed supercell size, E_b appears to exhibit decaying oscillatory variation with a period of 3 ML. However, the phase of this oscillation is reversed between the two supercells, and there is no simple Schulte-type explanation of such behavior. One possible explanation is the stacking periodicity of the films.

The significant difference between results obtained using (3×3) and (4×4) supercells immediately suggests that the assumption of a cutoff distance of $2a$ (where again a denotes the surface lattice constant) is not justified for pairwise interactions on Ag(111). It is tempting to include longer-ranged interactions within a lattice-gas (LG) model formalism in order to rederive the NN interactions as well as to extract longer-range interactions from DFT results. Given the limited number of configurations and poor convergence of results, this exercise is not very successful. As an aside, an analysis of dependence on supercell size has been performed previously for slab thickness $L=5$.[48]

Similarly, on Cu(111) films, the NN interaction energy for Cu adatoms is also sensitive to the lateral size of the supercell. Due to relative small number of k points used in the calculations, we cannot discern any particular pattern in QSE. The bulk values (with both bulk terminated and relaxed configurations) deduced by averaging results from $L=8$ to 15 are listed in Table I. Results using the larger (4×4) supercells are significantly lower than those using (3×3) supercells (Fig. 5).

IV. ADATOM AND VACANCY FORMATION ENERGIES

A precise definition of the formation energy, $E_f>0$, for an adatom (introduced briefly in Sec. I) is the energy cost to transfer that adatom from a 2D condensed island phase to the terrace. It is convenient to define a chemical potential, $\mu(L)$, for adatoms in the 2D condensed phase adsorbed on top of a slab of thickness L. When evaluated using an $(m\times m)$ supercell, this quantity is given by

$$\mu^m(L) = [E_0^m(L+1) - E_0^m(L)]/N_A, \tag{4}$$

where N_A is the number of surface atoms on one side of the slab in a supercell. Then, the formation energy for an adatom

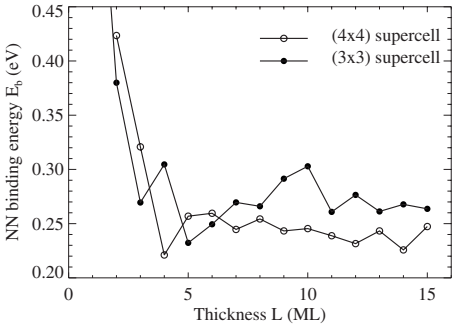

FIG. 5. NN pair interaction between Cu adatom on Cu(111). The solid circles are derived from using (3×3) supercells with a (4×4) k-point grid. The open circles are derived from using (3×3) supercells and a (4×4) k-point grid.

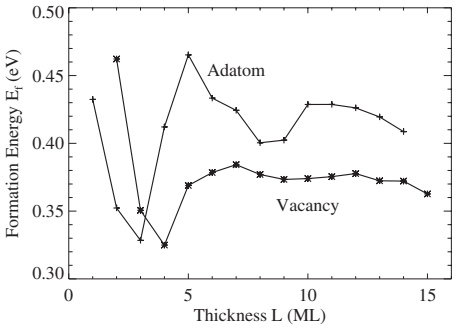

FIG. 6. Formation energy for a single Ag adatom and single vacancy on Ag(100), obtained using Eq. (5) with (3×3) supercells and (8×8) k points.

on a slab of thickness L is obtained from DFT energetics via

$$E_f^a(L) = -E_a(L) - \mu^m(L) = E_1^m(L) - E_0^m(L) - \mu^m(L), \quad (5)$$

where E_a is the relevant adatom adsorption energy defined in Eq. (1).

Another perspective is that $E_f^a(L)$ corresponds to the difference between the total energy of an adlayer with a condensed island of $M-1$ adatoms plus an isolated adatom, $-E_a(L)+(M-1)\mu(L)$, and the total energy of an island of M adatoms, $M\mu(L)$.

Next, we consider the formation energy, $E_f^v(L)$, for a vacancy on top of a slab of thickness $L-1$. This corresponds to the energy cost to incorporate a vacancy into the condensed phase on top this $(L-1)$-layer slab where the vacancy is taken from a vacancy pit within the same layer (or, equivalently, the adatoms displaced upon incorporating the vacancy remain in the same layer). Analogous to the above treatment for adatoms, $E_f^v(L)$ is given by the difference between the total adlayer energy for an island of M adatoms incorporating a vacancy and that for a vacancy-free island of M adatoms. The former is given by $dE_v(L)+(M+1)\mu(L-1)$ and the latter by $M\mu(L-1)$. Here, we set $dE_v(L)=E_v(L)-E_0(L)$, where $E_v(L)[E_0(L)]$ is the energy of the slab of thickness L with [without] a single vacancy in the top layer. Thus, $E_f^v(L)$ can be calculated from

$$E_f^v(L) = E_v^m(L) - E_0^m(L) + \mu^m(L-1) \quad (6)$$

using an $(m\times m)$ supercell.

Results for the dependence of slab thickness, L, of the formation energy for both adatoms and vacancies on Ag(100) is shown in Fig. 6. A large variation is found in E_f^a, similar to that of pair interaction E_b while E_f^v is relatively less sensitive to the film thickness for $L\geq1$. As for the adatom NN pair interaction, the adatom formation energy is much higher for $L=5$. Interestingly, for $L=2$ and $L=3$, the formation energy of a vacancy is higher than that of an adatom while for other film thickness, the opposite is true.

Analogous to the previous section, we have estimated the formation energies for a bulk homoepitaxial thin film by averaging DFT values for slabs ranging from $L=8$ to $L=15$. Results for both adatoms and vacancies on various Ag and Cu surfaces using (3×3) supercells are listed in Table II. Error estimates in the brackets are the standard deviations of

TABLE II. Formation energy of adatoms and vacancies on Ag and Cu surfaces. Results are derived from DFT calculations on (3×3) supercells and average over slabs with thickness ranging from $L=8$ to $L=15$.

	Adatom	Vacancy
Ag(100)	0.416(2)	0.373(1)
Ag(111)	0.601(1)	0.545(3)
Cu(100)	0.591(2)	0.505(3)
Cu(111)	0.800(3)	0.784(2)

results for various slab thicknesses divided by the number of samples. Note that for both Ag(100) and Cu(100) surfaces, the formation energy of an adatom is larger than that of an vacancy. This trend is consistent with the DFT-GGA results for Cu(100) of Klünker *et al.*[18] obtained about ten years ago. However, their values (0.48 eV for adatoms and 0.22 eV for vacancies) are significantly lower in magnitude than our present results (0.59 eV for adatoms and 0.50 eV for vacancies) for Cu(100). The discrepancy could be partly explained by the significant QSE observed for the (100) surfaces (especially around $L=4$.)

We find that a significant dependence of estimates for the formation energies on supercell size. To assess convergence with increasing size, for (100) surfaces we compare results for $(\sqrt{2}\times\sqrt{2})R45°$, (2×2), $(\sqrt{5}\times\sqrt{5})R26.6°$, $(2\sqrt{2}\times2\sqrt{2})R45°$, (3×3) and (4×4) supercells. For (111) surfaces, we compare $(\sqrt{3}\times\sqrt{3})R30°$, (2×2), $(\sqrt{7}\times\sqrt{7})R19.1°$, (3×3), $(2\sqrt{3}\times2\sqrt{3})R30°$, and (4×4) supercells. Note that the procedure of averaging over several slab thicknesses is essential to obtain a meaningful determination of supercell size effects since comparison between results for different supercells requires k-point convergence which is very difficult to achieve, a feature also observed for Ag/Ag(111) previously.[43] As shown earlier, averaging over results of different slab thicknesses improve k-point convergence tremendously. To systematically investigate supercell size effects, and to gain more insight to the question whether any such effects are electronic or elastic in nature, we carry out DFT calculations with all atoms fixed at their bulk termination positions (including the adatom, such as it is fixed above the substrate with a distance equal to the bulk interlayer spacing).

Figure 7(top) shows the deviation in the formation energy of Ag adatom on Ag(100) and Ag(111) surfaces from the value for the largest supercell calculated. For Ag(100), the formation energy on a $(\sqrt{2}\times\sqrt{2})R45°$ is much lower than that for larger supercells but then it quickly converges to the large-size limit. In contrast, on Ag(111), although the deviation in the formation energy for the smallest nonprimitive supercell is not as big as for the Ag(100) surface, the convergence to the large supercell limit is much slower, with significant effects of finite supercell size up to at least $4a$. Results for Cu(100) and Cu(111), also shown in Fig. 7(bottom), are similar. The main difference is that the deviation is about twice as large as for the Ag surfaces.

To interpret results shown in Fig. 7, we can analyze behavior of a LG model formalism with long-range interac-

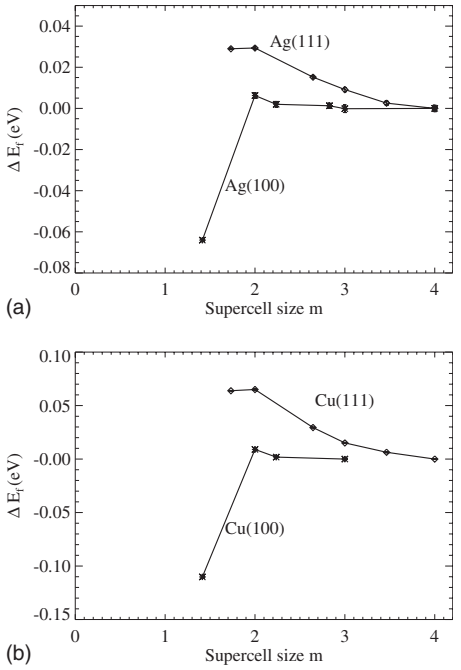

FIG. 7. Deviations in the formation energy of an adatom for different supercells. Results are for configurations with atoms (including adatoms) fixed at their bulk termination positions.

tions. If one neglects any many-body interactions and constructs a LG model with pairwise interactions only, then the difference in the adatom formation energy between a $(m \times m)$ supercell and a $(2m \times 2m)$ can be accounted for by an interaction of range m. Using results from Fig. 7, for Ag(100), there is 2NN (with $d=\sqrt{2}a$) attraction of 0.032 eV, and the interaction is less than 3 meV (which is the limit of our DFT accuracy) for larger separations. For Ag(111), there is a 0.009 eV repulsion between 2NN adatom pairs (with $d=\sqrt{3}a$), and also between 3NN adatom pairs (with $d=2a$). We do not have sufficient data to deduce directly the interaction for $d=\sqrt{7}a$, but from the available data, we expect it to be a repulsion of around 0.004 eV. Earlier studies on a compressed Ag(111) surface[42–44] show a stronger (around 0.050 eV) repulsion between adatoms, and a weaker repulsion for the unstrained Ag(111) surface,[42,43] consistent with the present study.

Similarly, we find a 0.055 eV attraction between 2NN adatom pairs on Cu(100), and that interactions beyond $2a$ drop below 3 meV. There is a 0.019 eV repulsion between 2NN adatom pairs on Cu(111) and a 0.021 eV repulsion between 3NN adatom pairs. The conclusion for Cu(100) is consistent with Ref. 37 but our results suggests a much stronger 2NN repulsion between adatoms (19 vs 1–4 meV), together with a much weaker NN attraction on Cu(111) (239 vs 323 meV) than Ref. 37. Low-temperature scanning tunnel microscope (STM) experiments of Cu/Cu(111) suggesting a repulsion between 0.010 and 0.019 eV have been reported.[49,50]

Note that the above results are for unrelaxed configurations, with all atoms (including adatoms) fixed at their bulk termination positions. Thus, derived interactions neglect any elastic effects. However, limited results that do include relaxation show that most of the supercell size effects are captured by Fig. 7.

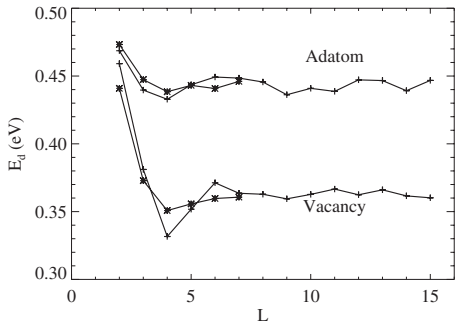

FIG. 8. Diffusion barriers for adatoms and vacancies on Ag(100). Average of thicknesses, L, from 9 to 15 gives 0.442(2) eV for adatom and 0.363(3) eV for vacancy. Data are for (3×3) supercell and a (4×4) k-point grid, shown as plus signs. Data using a (8×8) k-point grid are also shown as asterisks for comparison.

V. ADATOM AND VACANCY DIFFUSION BARRIERS

To determine diffusion barriers, we simply calculate the difference in energies between the different relevant high-symmetry sites for an adatom or vacancy. These are the hollow and bridge sites for our application, where for fcc(111) surfaces the fcc rather than the hcp hollow site is relevant having a slightly lower energy. While it is possible that the bridge site represents a (weak) local minimum in the energy landscape rather than the true transition state for hopping, any additional barrier should be very small.

Figure 8 shows the hopping barrier for an adatom and advacancy on Ag(100). In contrast to the binding energy and formation energy, there is no significant QSE once the slab thickness is above five layers. Table III lists the hopping barriers of an adatom and vacancy on the (100) and (111) surfaces of Ag and Cu.

The value for E_d on Ag(111) is significantly lower than the previous DFT estimate of 0.082 eV in Ref. 16 and experimental estimate 0.097 eV.[35] With such low-energy barriers, there are many factors that can affect the precise estimate of the diffusion barrier. We find that relaxation of the substrate is very important. For example, with a four-layer slab, (2×2) supercell, and (6×6) k-point grid (including the Γ point), the diffusion barrier is, respectively, 0.093, 0.057, and 0.055 eV with zero, one, and three layers of substrate fully relaxing. Similarly, for adatom diffusion on Cu(111), the barrier ranges from 0.042 eV with full substrate relaxation to 0.12 eV with no substrate relaxation.

Experiments of Ag and Pt(111),[35] effective-medium theory,[35] and DFT (Ref. 16) all show that the diffusion bar-

TABLE III. Hopping barriers for a single adatom and vacancy. Results are obtained from an average for slab thickness from $L=8$ to $L=15$, unless otherwise noted.

	Adatom$^{2\times2}$	Adatom$^{3\times3}$	Vacancy$^{3\times3}$
Ag(100)	0.440(2)	0.442(1)	0.363(1)
Ag(111)	0.052(1)[a]	0.059(3)	0.518(3)
Cu(100)	0.542(1)		0.405(6)
Cu(111)	0.046(1)[a]		

[a]Average of $L=5-9$.

TABLE IV. Energy barrier E_d (in eV) for adatom diffusion on Ag(111), calculated with different *xc* functionals and lattice constants a_0. Results are obtained with (2×2) supercells, $(12\times12\times1)$ *k*-point grid, and 250 eV energy cutoff, averaging over values from $L=5$ to 9. Numbers in brackets are obtained with the same setting except for a larger energy cutoff of 400 eV. Bold face numbers are for the unstrained surface. Two sets of potentials are used.

		PAW-std	
a_0 (Å)	4.017	4.069	4.169
LDA	**0.064(0.068)**	0.076(0.081)	
PBEsol		**0.057(0.061)**	
PBE		0.027(0.037)	**0.052(0.056)**
		PAW-new	
a_0 (Å)		4.055(4.053)	4.152(4.147)
PBEsol		**0.056(0.060)**	
PBE			**0.052(0.052)**

rier on Ag(111) is very sensitive to strain. Because of the relative large discrepancy of the theoretical lattice constant using PBE and the experimental value, it is perhaps warranted to examine other GGA methods with different theoretical lattice constants (see Appendix for more details). Table IV shows the adatom diffusion barrier E_d for Ag(111) calculated with different *xc* functionals and lattice constants. For unstrained surfaces, we have $E_d(\text{LDA})>E_d(\text{PBEsol})>E_d(\text{PBE})$, similar to the trend seen in the cohesive energy. Note that PBEsol predictions for both the lattice constant and the cohesive energy, perhaps the two most important factors determining the diffusion coefficient, are quite accurate compared with experiments.[26] To gauge the effect of pseudopotentials, we also perform calculations with a different PAW (denoted by PAW-new) potentials with improved treatment of *f* channels.[34] Results are essentially the same as the standard potential (PAW-std).

From experimentally observed island densities at low temperature during submonolayer homoepitaxy on Ag(111), a diffusion barrier of 97 ± 10 meV with a prefactor of 2×10^{11} is deduced[4,35] using the classic theory of irreversible island formation. However, in similar system such as 1 ML Ag/Pt(111) (Ref. 42) and Cu/Cu(111),[39,50,51] application of the classic theory produced artificially low diffusion rates (specifically, low prefactors if adopting standard choice of barriers). This anomaly was attributed to the presence of a "repulsive ring" around adatom inhibiting the approach of other adatoms. Based on the reasonable agreement with experiment of the previously reported DFT value of 0.082 eV for the diffusion barrier of Ag on unstrained Ag(111) (with local-density approximation (LDA) and a lattice constant 4.05 Å,[16] see Table IV also), it is concluded[52] that the repulsive interactions between adatoms was weak. This conclusion was consistent with previous DFT analysis.[42] However, in the light of our new lower value of E_d for Ag on Ag(111), this picture should be reexamined. Current DFT calculations do not produce a resolution to this issue.

Note that the current value of 0.042 eV for adatom diffusion for Cu on Cu(111) is more consistent with previously reported values, either from direct STM measurement of the hop rate[40,49] or DFT calculations.[39] It should also be noted that our new lower value of diffusion barrier for Ag on Ag(111) seems more consistent with this result for Cu. This claim is based on the general belief that surface energetics at least to some extent reflect the bulk cohesive energy which is actually higher for Cu than for Ag.[53]

Our calculation shows that on Ag(100) and Cu(100), the vacancy diffusion barrier is lower than the barrier for adatom diffusion. (All barriers apply for a hopping mechanism since exchange processes are less facile.) This trend for adatom versus vacancy diffusion barrier is consistent with previous results obtained by Klünker *et al.*[18] for the Cu(100) surface (just as trends in our results for the formation energies were consistent with theirs). Note that here QSE is not very significant so as a consequence values in Ref. 18 (0.52 eV for adatoms and 0.42 for vacancies) are basically consistent with our present values. Recall that the effective barrier for coarsening is given by the sum of the diffusion barrier and formation energy for the adspecies transporting mass, plus any additional attachment barrier. Together with the result that the formation energies for vacancies is lower than for adatoms, the lower diffusion barrier for vacancies gives credence to the picture proposed previously based on experimental observations that vacancies are the dominant mass transport species for adatom island ripening at 340 K on Cu(100).[54] However, the remaining uncertainty is the magnitude of the additional barrier for interlayer attachment of a vacancy to a step edge compared with the (zero) additional barrier of intralayer adatom attachment.

It is reasonable to question also whether the lateral size of the supercell has any significant effect on the hopping barrier. Our data suggest that those effects are quite small.

VI. DISCUSSION AND CONCLUSIONS

DFT is currently the de facto standard for *ab initio* calculation of surface energetics. However, even for systems as simple as the (100) and (111) surfaces of Ag and Cu, considerable uncertainties remain concerning the values of key energetics, such as NN binding energy of adatoms, adatom, and vacancy formation energies, etc.

From extensive calculations with different slab thicknesses and supercell sizes, we show that within the theory and a fixed form of exchange-correlation approximation, much of the uncertainties can be explained by two types of finite-size effects.

For (100) surfaces, the slab thickness is important as a consequence of the confinement of electrons within the slab.[46] Reliable estimates for surface energetics in the limit of bulk films usually requires slab thickness above ten layers. On the other hand, for (111) surfaces, the supercell size is more important, a feature which likely arises from the long-range interactions induced by the surface states. Perhaps a good gauge of this range is the half in-plane Fermi wavelength, which is about six surface lattice constants for Ag(111), and four surface lattice constants for Cu(111), the predicted period of oscillations in adatom interactions induced by the surface state.[38]

Another limiting factor for plane-wave DFT calculations is the number of k points used for integrating the surface Brillouin zone. We find the k-point convergence is very difficult to achieve with a fixed slab thickness, requiring up to a (60×60) k-point grid for a primitive surface cell to converge within a few meV. The slow convergence is also found for Al(110) and is believed due to inadequate sampling of surface states near the Fermi level.[55] However, empirically, the average value of results for several slab thickness converge much faster. Therefore, the systematic study of effects of slab thicknesses has the additional benefit of achieving faster k-point convergence.

It is worth noting that the real challenge in *ab initio* calculations of surface energetics is still with the theory itself, which currently focus on better forms of approximations of the exchange-correlation functional in DFT. Results with different approximations are discussed briefly in Appendix. We note that effects of slab thicknesses are basically transferable, i.e., the QSE curve in Figs. 2–6 are shifted by a near constant value for different functionals. However, it has been shown that the position of the surface state relative to the Fermi energy is very sensitive to the equilibrium bulk constant,[14,44] which is in turn sensitive to the functional. Thus, effect of long-range interactions may be more sensitive to the choice of functionals.

ACKNOWLEDGMENTS

The author wishes to thank J. W. Evans for extensive discussions and inputs on the implication of the energetics calculated and the manuscript, also G. Kresse and J. Paier for advice on the PAW potentials. This work was supported by the U.S. Department of Energy (USDOE), Basic Energy Sciences—Division of Chemical Sciences. The work was performed at Ames Laboratory which is operated for the USDOE by Iowa State University under Contract No. DE-AC02-07CH11358. Computations were partly performed with NERSC resources.

APPENDIX: COMPARISON BETWEEN DIFFERENT *xc* FUNCTIONALS

All DFT results presented above were obtained from the widely used PBE form[23] of exchange-correlation functional. In terms of qualitative trends regarding effects of film thickness, we do not find any significant difference when other functionals are used. However, the absolute values of energies are sensitive to the functionals. For a wide range of transition metals, LDA underestimate the lattice constant while PBE overestimate the lattice constant. PBE generally predicts weaker binding energy between atoms than LDA.

Designing improved functionals that uniformly give better predictions without any adjustable parameter is very difficult. Recently, several new functionals, e.g., Wu-Cohen,[31] AM05,[56] and PBEsol (Ref. 57) are introduced which show improvements over LDA and PBE in their predictions of bulk properties (lattice constants and bulk modulus).[26] In this section, we compare results of LDA, PBE, and PBEsol for the lattice constant, the free energy of clean surfaces, and the formation energy for a single adatom on Ag(100) and Cu(100). This provides some assessment of effects of the choice of exchange-correlation functionals.

TABLE V. Comparison between DFT predictions for the lattice constant a_0, the surface energy γ, and adatom formation energies for select Ag and Cu surfaces, using various exchange-correlation functional. Results for E_f^a are obtained using (2×2) supercells with all atoms fixed at their bulk positions. Results for surfaces are averages over slab thicknesses from $L=8$ to $L=15$. Experimental values for lattice constants are based on room-temperature values corrected to the $T=0$ limit, from Ref. 30. Experimental values for surface energies are from Ref. 62. PAW-std are the pseudopotentials included in the VASP package while PAW-new are new pseudopotentials with improved treatment of the f channel (Ref. 34). See text for more technical details.

	LDA	PBEsol	PBE	Expt.
		Lattice constant (Å)		
Ag(PAW-std)	4.017	4.069	4.169	4.056
Ag(PAW-new)		4.055	4.153	
Cu(PAW-std)	3.524	3.570	3.637	3.595
Cu(PAW-new)		3.571	3.636	
		Surface energy γ		
Ag(111) PAW-std				
eV/atom	0.505	0.449	0.341	0.535
J/m^2	1.158	1.002	0.726	1.250
Ag(111) PAW-new				
eV/atom		0.442	0.341	
J/m^2		0.995	0.733	
Cu(111) PAW-std				
eV/atom	0.600	0.556	0.463	0.610
J/m^2	1.789	1.614	1.294	1.825
		Formation energy (unrelaxed) (eV)		
Ag/Ag(100)	0.743(4)	0.654(5)	0.515(3)	
Cu/Cu(100)	0.911(9)	0.850(4)	0.716(4)	

Large-scale surface energetics calculations necessitate the usage of pseudopotentials that treat some electrons as frozen cores. Although for most bulk properties, the PAW method predicts values very close to that of full potential methods, there can be noticeable differences in surface energetics.[34] Here we compare results using the "standard" PAW potentials that are included in the VASP package (PAW-std) and a set of new PAW potentials with improved treatment of f channels (PAW-new).

All lattice constants are obtained from quadratic fitting of results ±0.02 Å from the theoretical equilibrium value, with $(24\times24\times24)$ (including the Γ point) k-point grid and 250 eV energy cutoff. Some differences in the lattice constant can be observed when the energy cutoff is increased to 600 eV but they are not very significant.

The surface energy is defined as through

$$\gamma(L) = [E_0(L) - L\sigma_b]/(2A), \quad \text{(A1)}$$

where $E_0(L)$ is the energy of a film of L-layer thickness, σ_b is the cohesive energy per atom, and A is the area (per side) of the unit cell. $E_0(L)$ are calculated using periodic slabs separated by 12 Å of vacuum, using $(24\times24\times1)$ (including the Γ-point) k-point grid. In the literature, two general methods of estimating σ_b has been used. The first method is to obtain σ_b from a separate calculation. This can be either from a simple bulk calculation using the primitive cell, and the more sophisticated method of filling up the vacuum between slabs with additional layer of atoms, as investigated by Fiorentini and Methfessel.[58] This method has been criticized[58,59] as unreliable but recently argued by Da Silva, Stampfl, and Scheffler[60] as valid if one is careful when choosing the setting of the bulk calculation. The alternative method is to use a linear fit to the total energy of varying slab thickness as σ_b. I find that although, in principle, this is a more reliable (and perhaps more foolproof) method for very large L, due to QSE, for L up to 12 ML, a more judiciously chosen σ_b sometimes gives better results.

In this appendix, σ_b is also calculated from a slab calculation. However, instead of filling up the vacuum as suggested by Fiorentini and Methfessel,[58] the distance between the two slabs is shrunk to the interlayer distance to recover the bulk property. So for (111) surfaces, a supercell with three atoms and a $(24\times24\times10)$ k-point grid is used for the cohesive energy calculation. It should be more accurate than using the bulk cohesive energy of a fcc primitive cell since the k-point distributions there are not equivalent with the slab calculation, even though they are describing the same physical system. Using the very high-quality data in Ref. 61 for Ag(100) with a $(51\times51\times1)$ k-point grid up to $L=31$ ML as a benchmark, I find that this method is slightly (about 5 meV/atom) more accurate than the method of linear fit using data up to $L=15$ ML. For all three quantities calculated, results for PBEsol lie between the LDA values and the PBE values (Table V). Our results for the lattice constants is in good agreement with previous DFT calculations. In particular, using PAW-new potentials, our results are in complete agreement with those published in Ref. 26 for the same functional and potential. Our PBE value of $\gamma=0.463$ eV/atom for Cu(111) is in very good agreement with Da Silva *et al.*[63] (0.468 eV/atom) and Stasevich *et al.*[37] 0.462–0.465 eV/atom but slightly different from the value 0.48 eV/atom of Tran *et al.*[64] Tran *et al.*[64] calculated the surface energies for various metals using LDA, PBE, and Wu-Cohen (WC) *xc* functionals. Our results for Ag and Cu with LDA and PBE are in good agreement with their results. Our results with PBEsol are in good agreement with the WC results for the two metals studied here. However, this is a small systematic difference of around 0.02 eV/atom.

[1] P. Ruggerone, C. Ratsch, and M. Scheffler, in *The Chemical Physics of Solid Surfaces*, Growth and Properties of Ultrathin Epitaxial Layers Vol. 8, edited by D. A. King and D. P. Woodruff (Elsevier, Amesterdam, 1997), p. 490.

[2] *MRS Bulletin*, Density Functional Theory in Materials Research Vol. 31, edited by C. Wolverton, J. Hafner, and G. Ceder (Materials Research Society, Pittsburg, 2006).

[3] T. Michely and J. Krug, *Islands, Mounds, and Atoms* (Springer, Berlin, 2004).

[4] J. W. Evans, P. A. Thiel, and M. C. Bartelt, Surf. Sci. Rep. **61**, 1 (2006).

[5] M. C. Bartelt, L. S. Perkins, and J. W. Evans, Surf. Sci. Lett. **344**, L1193 (1995).

[6] C. Busse, W. Langenkamp, C. Polop, A. Petersen, H. Hansen, U. Linke, P. J. Feibelman, and T. Michely, Surf. Sci. Lett. **539**, L560 (2003).

[7] P. A. Thiel and J. W. Evans, J. Phys. Chem. B **108**, 14428 (2004).

[8] M. Li, P.-W. Chung, E. Cox, C. J. Jenks, P. A. Thiel, and J. W. Evans, Phys. Rev. B **77**, 033402 (2008).

[9] J. Tersoff, A. W. Denier van der Gon, and R. M. Tromp, Phys. Rev. Lett. **72**, 266 (1994).

[10] J. Rottler and P. Maass, Phys. Rev. Lett. **83**, 3490 (1999).

[11] J. Krug, P. Politi, and T. Michely, Phys. Rev. B **61**, 14037 (2000).

[12] K. Morgenstern, Phys. Status Solidi B **242**, 773 (2005).

[13] P. A. Thiel, M. Shen, D.-J. Liu, and J. W. Evans, J. Phys. Chem. C **113**, 5047 (2009).

[14] G. Neuhold and K. Horn, Phys. Rev. Lett. **78**, 1327 (1997).

[15] B. D. Yu and M. Scheffler, Phys. Rev. B **55**, 13916 (1997).

[16] C. Ratsch, A. P. Seitsonen, and M. Scheffler, Phys. Rev. B **55**, 6750 (1997).

[17] G. Boisvert and L. J. Lewis, Phys. Rev. B **56**, 7643 (1997).

[18] C. Klünker, J. B. Hannon, M. Giesen, H. Ibach, G. Boisvert, and L. J. Lewis, Phys. Rev. B **58**, R7556 (1998).

[19] G. Kresse and J. Hafner, Phys. Rev. B **47**, 558 (1993).

[20] G. Kresse and J. Hafner, Phys. Rev. B **49**, 14251 (1994).

[21] G. Kresse and J. Furthmüller, Phys. Rev. B **54**, 11169 (1996).

[22] G. Kresse and J. Furthmüller, Comput. Mater. Sci. **6**, 15 (1996).

[23] J. P. Perdew, K. Burke, and M. Ernzerhof, Phys. Rev. Lett. **77**, 3865 (1996).

[24] P. E. Blöchl, O. Jepsen, and O. K. Andersen, Phys. Rev. B **49**, 16223 (1994).

[25] G. Kresse and D. Joubert, Phys. Rev. B **59**, 1758 (1999).

[26] G. I. Csonka, J. P. Perdew, A. Ruzsinszky, P. H. T. Philipsen, S. Lebègue, J. Paier, O. A. Vydrov, and J. G. Ángyán, Phys. Rev. B **79**, 155107 (2009).

[27] P. Haas, F. Tran, and P. Blaha, Phys. Rev. B **79**, 085104 (2009).

[28] C. Kittel, *Introduction to Solid State Physics*, 8th ed. (Wiley, New York, 2004).

[29] A. Khein, D. J. Singh, and C. J. Umrigar, Phys. Rev. B **51**, 4105 (1995).

[30] V. N. Staroverov, G. E. Scuseria, J. Tao, and J. P. Perdew, Phys. Rev. B **69**, 075102 (2004).

[31] Z. Wu and R. E. Cohen, Phys. Rev. B **73**, 235116 (2006).

[32] J. Paier, M. Marsman, K. Hummer, G. Kresse, I. C. Gerber, and J. G. Ángyán, J. Chem. Phys. **124**, 154709 (2006).

[33] A. E. Mattsson, R. Armiento, J. Paier, G. Kresse, J. M. Wills,

and T. R. Mattsson, J. Chem. Phys. **128**, 084714 (2008).
[34] A. Kiejna, G. Kresse, J. Rogal, A. De Sarkar, K. Reuter, and M. Scheffler, Phys. Rev. B **73**, 035404 (2006).
[35] H. Brune, K. Bromann, H. Röder, K. Kern, J. Jacobsen, P. Stoltze, K. Jacobsen, and J. Nørskov, Phys. Rev. B **52**, R14380 (1995).
[36] T. L. Einstein, in *Physical Structure*, Handbook of Surface Science Vol. 1 (Elsevier, Amsterdam, 1996), p. 577.
[37] T. J. Stasevich, T. L. Einstein, and S. Stolbov, Phys. Rev. B **73**, 115426 (2006).
[38] P. Hyldgaard and M. Persson, J. Phys.: Condens. Matter **12**, L13 (2000).
[39] A. Bogicevic, S. Ovesson, P. Hyldgaard, B. I. Lundqvist, H. Brune, and D. R. Jennison, Phys. Rev. Lett. **85**, 1910 (2000).
[40] J. Repp, F. Moresco, G. Meyer, K.-H. Rieder, P. Hyldgaard, and M. Persson, Phys. Rev. Lett. **85**, 2981 (2000).
[41] V. S. Stepanyuk, A. N. Baranov, D. V. Tsivlin, W. Hergert, P. Bruno, N. Knorr, M. A. Schneider, and K. Kern, Phys. Rev. B **68**, 205410 (2003).
[42] K. A. Fichthorn and M. Scheffler, Phys. Rev. Lett. **84**, 5371 (2000).
[43] K. A. Fichthorn and M. Scheffler, in *Collective Diffusion on Surfaces: Correlation Effects and Adatom Interactions*, NATO Science Series II. Mathematics, Physics and Chemistry Vol. 29, edited by M. C. Tringides and Z. Chvoj (Plenum, Dordrecht, 2001).
[44] W. Luo and K. A. Fichthorn, Phys. Rev. B **72**, 115433 (2005).
[45] C. M. Wei and M. Y. Chou, Phys. Rev. B **68**, 125406 (2003).
[46] F. K. Schulte, Surf. Sci. **55**, 427 (1976).
[47] Y. Han, J. W. Evans, and D.-J. Liu, Surf. Sci. **602**, 2532 (2008).
[48] For Ag, (111) using slabs with $L=5$, one finds that $E_b=0.233$, 0.153, 0.229, 0.200, and 0.196 for $(m\times m)$ supercells with $m=2-6$, respectively, and a $(n\times n\times 1)$ k-point selection with $n=12,6,4,4,2$, respectively. See M. Shen, J.-M. Wen, C. J. Jenks, P. A. Thiel, D.-J. Liu, and J. W. Evans, Phys. Rev. B **75**, 245409 (2007).
[49] N. Knorr, H. Brune, M. Epple, A. Hirstein, M. A. Schneider, and K. Kern, Phys. Rev. B **65**, 115420 (2002).
[50] J. A. Venables and H. Brune, Phys. Rev. B **66**, 195404 (2002).
[51] C. Ratsch and J. A. Venables, J. Vac. Sci. Technol. A **21**, S96 (2003).
[52] C. Ratsch and M. Scheffler, Phys. Rev. B **58**, 13163 (1998).
[53] P. J. Feibelman, Surf. Sci. **423**, 169 (1999).
[54] J. B. Hannon, C. Klünker, M. Giesen, H. Ibach, N. C. Bartelt, and J. C. Hamilton, Phys. Rev. Lett. **79**, 2506 (1997).
[55] K. M. Ho and K. P. Bohnen, Phys. Rev. B **32**, 3446 (1985).
[56] R. Armiento and A. E. Mattsson, Phys. Rev. B **72**, 085108 (2005).
[57] J. P. Perdew, A. Ruzsinszky, G. I. Csonka, O. A. Vydrov, G. E. Scuseria, L. A. Constantin, X. Zhou, and K. Burke, Phys. Rev. Lett. **100**, 136406 (2008).
[58] V. Fiorentini and M. Methfessel, J. Phys.: Condens. Matter **8**, 6525 (1996).
[59] J. C. Boettger, Phys. Rev. B **49**, 16798 (1994).
[60] J. L. F. Da Silva, C. Stampfl, and M. Scheffler, Surf. Sci. **600**, 703 (2006).
[61] Y. Han and D.-J. Liu, Phys. Rev. B **80**, 155404 (2009).
[62] F. R. de Boer, R. Boom, W. C. M. Mattens, A. R. Miedema, and A. K. Niessen, *Cohesion in Metals: Transition Metal Alloys*, Cohesion and Structure Vol. 1 (North-Holland, Amsterdam, 1988).
[63] J. L. F. Da Silva, C. Barreteau, K. Schroeder, and S. Blügel, Phys. Rev. B **73**, 125402 (2006).
[64] F. Tran, R. Laskowski, P. Blaha, and K. Schwarz, Phys. Rev. B **75**, 115131 (2007).